Experimental Verification of the Petroelastic Model in the Laboratory - Fluid Substitution and Pressure Effects.

Patrick Rasolofosaon, Bernard Zinszner

Oil & Gas Science and Technology – Rev. IFP Energies nouvelles, Vol. 67 (2012), No. 2, pp. 303-318

DOI: 10.2516/ogst/2011167

Experimental Verification of the Petroelastic Model in the Laboratory – Fluid Substitution and Pressure Effects

P.N.J. Rasolofosaon and B. Zinszner

IFP Energies nouvelles, 1-4 avenue de Bois-Préau, 92852 Rueil-Malmaison Cedex - France
e-mail: patrick.rasolofosaon@ifpen.fr - bernard_zinszner@hotmail.com

Résumé — Vérification expérimentale du modèle pétroélastique au laboratoire – Substitutions de fluides et effets de pression — Le modèle poroélastique est une composante centrale dans les *workflows* permettant l'interprétation des données de sismique répétitive (ou sismique 4D) en vue de mettre en évidence les mouvements de fluide et/ou les variations de pression lors de l'exploitation des réservoirs. Ce modèle doit prendre en compte à la fois les effets de substitution de fluides et les effets de variation de pression sur les paramètres sismiques mesurés (vitesses, impédances). Cet article décrit une vérification expérimentale au laboratoire de ce modèle. Concernant les effets de substitution de fluides, le modèle de Biot-Gassmann est le plus utilisé. Ce modèl considère que le module de cisaillement est indépendant de la nature du fluide saturant, quand celui-ci est non visqueux, et relie les variations des modules d'incompressibilité de la roche due à la substitution de fluides aux paramètres du milieu poreux et des fluides saturants. La validation expérimentale, portant donc sur les deux aspects, montre sur un échantillonnage varié de grès et de calcaires poreux que le module de cisaillement de la roche est indépendant du fluide saturant peu visqueux. Cette indépendance est vérifiée, même dans le cas de fluides visqueux (viscosité inférieure à 10^4 cP), si la pression différentielle est élevée (fermeture des microfissures) ; l'écart entre le module d'incompressibilité mesuré et calculé est toujours faible ; le module d'incompressibilité des cristaux formant une roche monominérale (calcaire, grès propre) déduit de la formule de Gassmann est proche des valeurs données dans la littérature pour ces minéraux ; lors de mesures sous une même pression différentielle, mais avec des pressions de pore différentes, les écarts observés sur les modules d'incompressibilité sont comparables à ceux prévu par la formule de Biot-Gassmann en prenant en compte la variation du module d'incompressibilité du fluide saturant sous l'effet de la pression de pore (non linéarité). Ces trois dernières observations convergent vers la validation de la formule de Biot-Gassmann pour le module d'incompressibilité. Concernant les effets de pression, le paramètre pertinent est la pression différentielle $P_{diff} = P_c - P_p$, c'est-à-dire la différence entre la pression de confinement P_c et la pression de pore P_p. Plus précisément, nous démontrons que les vitesses des ondes *P* et *S* dépendent uniquement de la pression différentielle P_{diff}, et non individuellement des pressions P_c et P_p. Cette pression, en contribuant à fermer les micro-défauts mécaniques (contacts entre grains, microfissures), a des conséquences très variables sur les vitesses et les atténuations, suivant l'abondance relative de ces micro-défauts. Les roches calcaires, quelle que soit la pression, sont souvent très peu sensibles à cet effet, à cause de la facilité avec laquelle le carbonate cimente les micro-défauts. Les grès consolidés sont souvent sensibles à la pression différentielle et les roches inconsolidées (sables) très sensibles. La relation Vitesse *vs* P_{diff} est généralement du type loi puissance et l'exposant de cette relation est un excellent moyen de quantifier la sensibilité d'une roche à la pression.

Abstract — Experimental Verification of the Petroelastic Model in the Laboratory – Fluid Substitution and Pressure Effects *— The poroelastic model is a major component in the workflows for the interpretation of time-lapse (or 4D) seismic data in terms of fluid repartition and/or pressure variation during the exploitation of reservoirs. This model must take into account both the fluid substitution effect and the pressure variation effect on the measured seismic parameters (velocities, impedance). This paper describes an experimental verification in the laboratory of this model. Regarding fluid substitution, Biot-Gassmann model is the most popular model. This model assumes that the shear modulus is independent of the nature of the saturating fluid, as long as this latter is not viscous and give the expression of the variations of the bulk modulus of the rock due to fluid substitution as function of the parameters of the rock frame and of the saturating fluids. The experimental validation, dealing with these two items, demonstrates on various samples of sandstone and limestone that the shear modulus of the rock is independent of the not too viscous saturating fluid. This is verified even with viscous fluids (viscosity as large as 10^4 cP) if the differential pressure, that is to say the difference between the confining pressure and the pore pressure, is high (closure of the mechanical defects); the bulk modulus of the crystal constituent of mono-mineral rocks (limestone, clean sandstone) is close to tabulated values; under fixed differential pressure but variable pore and confining pressures, the variation of the rock bulk modulus can be explained by the nonlinearity of the fluid bulk modulus. These three types of experimental results constitute unambiguous corroborations of Biot-Gassmann theory. Regarding pressure effects, the relevant parameter is the differential pressure $P_{diff} = P_c - P_p$, that is to say the difference between the confining pressure P_c and the pore pressure P_p. More precisely, this means that P-wave and S-wave velocities only depend on the differential pressure $P_{diff} = P_c - P_p$, and not in an independent way on P_c and on P_p. Increasing the differential pressure P_{diff} tends to stiffen the rock by closing the mechanical defects (grain contacts, microcracks, microfractures...). The consequence on velocities and attenuations is variable according to the relative abundance of these mechanical defects in the rock sample. Limestones are often weakly pressure dependent, whatever the pressure level. This is due to the ease with which mechanical defects can be cemented by carbonate crystals. Consolidated sandstones are often sensitive to the differential pressure P_{diff} and the unconsolidated geomaterials (sands) are very pressure sensitive. The pressure dependence of the velocities is often well approximated by a power law. The exponent of this power law, often called the Hertz exponent, is a good way to quantify the pressure sensitivity of the rock velocities.*

INTRODUCTION

The correct interpretation of the time-lapse seismic data during the exploitation of reservoirs rests on the availability of a relevant petroelastic model that is able to correctly describe the simultaneous effect of fluid substitution and pressure variations on seismic properties (*e.g.*, Calvert, 2005). Here, we report experimental verification in the laboratory of the two most popular petroelastic models, namely Biot-Gassmann's poroelastic theory for describing fluid substitution effects (*e.g.*, Bourbié *et al.*, 1987) and Hertz-Mindlin theory for describing the pressure dependence of the seismic velocities (*e.g.*, Mavko *et al.*, 1988).

The paper is divided in four parts. First, we introduce both underlying theories. Then, we describe the experimental results regarding fluid substitution. Experimental results on the pressure dependence of the velocities are shown in the third section. Finally, the paper ends with some concluding remarks.

1 THEORETICAL ASPECTS

The macroscopic stress-strain laws of an isotropic porous medium saturated by a single fluid can be found for instance in Bourbié *et al.* (1987):

$$\sigma_{ij} = \left(K^{(dr)} - \frac{2}{3}\mu \right) Tr\,\varepsilon \times \delta_{ij} + 2\mu\varepsilon_{ij} - \alpha p \delta_{ij} \qquad (1)$$

$$p = M(\varsigma - \alpha \times Tr\,\varepsilon) \qquad (2)$$

where σ_{ij} and ε_{ij} are the components of the average increments of the stress tensor and strain tensor, respectively, over a Representative Elementary Volume (or REV) Ω of the porous medium. $Tr\,\varepsilon$ designates the trace of strain tensor and δ_{ij} the components of the unit symmetric tensor of rank 2, or Kronecker tensor ($\delta_{ij} = 1$ if $i = j$ and $\delta_{ij} = 0$ if $i \neq j$). The parameter p is the pore pressure increment over the pore volume part $\Omega^{(fl)}$ of the REV. If $\mathbf{u}$ and $\mathbf{U}$ are respectively the mean macroscopic overall displacement and the mean displacement of the fluid phase both over the REV Ω of the porous

medium, the increase of fluid content ς over Ω is defined by (Bourbié *et al*., 1987):

$$\varsigma = -\phi\, div(\mathbf{U} - \mathbf{u}) \tag{3}$$

where ϕ designates the porosity and *div* the divergence of the considered vector. Equations (1) and (2) are the most general linear isotropic equations linking the dynamic parameters, namely the stress σ_{ij} and the pore pressure p, and the kinematic parameters, namely the strain ε_{ij} and the increase of fluid content ς.

The physical interpretation of the additional physical constants is the following.

First, let us consider a "drained experiment", for which the pore pressure is kept constant in the pore volume part $\Omega^{(fl)}$ of the REV of the porous medium, that is to say $p = 0$ in Equation (1). Thus $K^{(dr)}$ and μ can be respectively interpreted as the bulk modulus and the shear modulus of the "drained" rock, the superscript (*dr*) standing for "drained".

The coefficient α in Equation (1) is related to the concept of effective stress for the bulk volumetric strain in the field of soil or rock mechanics (*e.g*., Bourbié *et al*., 1987; Coussy, 1995). In these contexts, if one corrects in Equation (1) the stress σ_{ij} by the quantity $\alpha p \delta_{ij}$ one obtains an alternative stress σ'_{ij}:

$$\sigma'_{ij} = \sigma_{ij} + \alpha p \tag{4}$$

satisfying the regular Hooke's stress-strain law. This alternative stress is nothing but the so-called "Biot effective stress" (*e.g*., Carroll, 1979; Bourbié *et al*., 1987; Thompson and Willis, 1987) and the dimensionless coefficient α is referred to as the Biot effective stress coefficient (Bourbié *et al*., 1987). The elastic coefficients $K^{(dr)}$ and μ and the dimensionless coefficient α only depend on the porous medium.

In Equation (2), the scalar M, which has the dimension of a pressure, is the only material constant which depends on the properties both of the porous medium and of the saturating fluid. Under the condition of non-deforming frame (*i.e*., $Tr\,\varepsilon = 0$), Equation (2) becomes:

$$p = M\varsigma \tag{5}$$

Thus, the coefficient M is the pressure to be exerted on the saturating fluid to increase the fluid content ς by a unit value in a non-deforming frame.

Now, let us consider an "undrained" experiment, in which the fluid content in a Representative Elementary Volume Ω of the porous medium is kept constant (*e.g*., Bourbié *et al*., 1987; Wang, 2000). This corresponds to the condition $\varsigma = 0$ in Equation (2). This leads to an expression of the pore pressure increment p which, when substituted in Equation (1), gives a new linear relation between the stress and the strain:

$$\sigma_{ij} = \left(K^{(dr)} + \alpha^2 M - \frac{2}{3}\mu\right) Tr\,\varepsilon \times \delta_{ij} + 2\mu\varepsilon_{ij} \tag{6}$$

where:

$$K^{(dr)} + \alpha^2 M = K^{(u)} \tag{7}$$

and μ can be straightforwardly interpreted as the bulk modulus and the shear modulus of the "undrained" rock, the superscript (*u*) standing for "undrained". Note the equality of the drained shear modulus and the undrained shear modulus, which implies the independence of the shear modulus of the rock with respect to the properties of the saturating fluid. This is one of the most important results of the poroelastic theory. The other important result is the link between the undrained bulk modulus $K^{(u)}$ and the drained bulk modulus $K^{(dr)}$ summarized by Equation (7).

Furthermore, Brown and Korringa (1975) and Gassmann (1997) give the link between the macroscopic parameters α and M of Equations (1, 2) and (7) and the microscopic parameters of the constituents (solid grain, fluid) and of the pore (porosity). Bourbié *et al*. (1987) give:

$$\alpha = 1 - \frac{K^{(dr)}}{K^{(gr)}} \tag{8}$$

$$\frac{1}{M} = \frac{\phi}{K^{(fl)}} + \frac{\alpha - \phi}{K^{(gr)}} \tag{9}$$

where $K^{(gr)}$ and $K^{(fl)}$ designate the bulk moduli of the grain constituent and of the saturating fluid, respectively. The two previous equations associated with Equation (7) are the famous Biot-Gassmann equations, widely used in fluid substitution problems of seismic monitoring (*e.g*., Calvert, 2005).

The link with the previous equations and the seismic waves is the following. Since seismic waves involve so quick processes that the fluid has no time to escape from the pores, it is often assumed that the experimentally measured wave moduli of the fluid-saturated rock are not very different from the undrained *P*- and *S*-waves moduli (Bourbié *et al*., 1987; Mavko *et al*., 1998) and are related to the undrained bulk and shear moduli by the relations:

$$\rho\left(V_P^{(sat)}\right)^2 = K^{(u)} + \frac{4}{3}\mu \;\; ; \;\; \rho\left(V_S^{(sat)}\right)^2 = \mu \tag{10}$$

where $V_P^{(sat)}$ and $V_S^{(sat)}$ are the ordinary *P*-wave and *S*-wave velocities and ρ the density of the fully saturated rock.

Up to now pressure dependence of the seismic velocities was not considered. Both confining pressure P_c and pore pressure P_p (not to be confused with the pore-pressure increment induced by the seismic wave) vary in the subsurface and modify any physical property of rocks. In the framework of an idealized rock-physics model, Gurevich (2004) demonstrated that seismic velocities essentially depends on the differential pressure $P_{diff} = P_c - P_p$ (the difference between the confining pressure P_c and the pore-pressure P_p) and not in an independent way on P_c and on P_p. This will be shown experimentally in the next sections.

One of the simplest model assumes a power law for the dependence of the velocities with the differential pressure P_{diff}:

$$\left(\frac{V_P(P_{diff\,1})}{V_P(P_{diff\,2})}\right)=\left(\frac{P_{diff\,1}}{P_{diff\,2}}\right)^{h_P} \text{ and } \left(\frac{V_S(P_{diff\,1})}{V_S(P_{diff\,2})}\right)=\left(\frac{P_{diff\,1}}{P_{diff\,2}}\right)^{h_S} \quad (11)$$

where $V_P(P_{diff\,i})$ and $V_S(P_{diff\,i})$ (i = 1, 2) are the P-wave an S-wave velocities, respectively, at the differential pressure $P_{diff\,i}$ (i = 1, 2). The exponents h_P and h_S of the power laws of Equation (11) are called the Hertz exponents, respectively of the P-wave velocity and of the S-wave velocity, with reference to the German physicist Heinrich Hertz who demonstrated by calculation that in a stack of isodiametral spheres, in elastic contact, velocity varies with the pressure according to a power law, and that for P-waves, the exponent is h_P = 1/6 (Mavko *et al*., 1998). In rocks Hertz exponents differ from this theoretical value. Experimental measurement of Hertz exponents in various types of rocks are reported in the next sections.

2 EXPERIMENTAL RESULTS ON FLUID SUBSTITUTION

2.1 Conventional Experimental Verification of the Petroelastic Model

Here, we illustrate the conventional procedure for experimentally checking the poroelastic equations of the previous section. First, P- and S-wave ultrasonic velocities on the "room dry" and on the saturated rock sample are measured by "first break" technique. The first break technique corresponds to the simplest and most common way to measure a velocity. It consists in picking the arrival time of the start (first break) of an acoustic signal which has propagated in the rock sample. The sample density ρ and the porosity φ are independently measured using conventional techniques (Bourbié *et al*., 1987). The fluid properties (density, bulk modulus) are either obtained from physical tables (Anderson, 1971; Batzle and Wang, 1992; Tamura *et al*., 1994; Daridon *et al*., 1999; Plantier *et al*., 2002) or also independently measured. Then, knowing the type of rock or analyzing the rock sample it is possible to identify the main mineral constituents and to give reasonable value for the bulk modulus and the density of the grain constituent (Bass, 1995; Zinszner and Pellerin, 2007). Some values are given in Table 1.

As previously said, the wave moduli of the saturated rock are identified with the undrained P- and S-waves moduli related to the undrained bulk and shear moduli by Equation (10).

Last, the drained bulk and shear moduli rock are wrongly identified with the bulk and shear moduli of the "room dry" rock in the literature, as clearly detailed by Mavko *et al*. (1998). This procedure has been checked on a large database (312 rock samples) available in the open literature.

We plot in Figure 1 the measured P-wave (figure on the left side) and S-wave (figure on the right side) ultrasonic velocities as functions of the corresponding undrained velocities using the Biot-Gassmann equations of the previous section. More precisely, the theoretical undrained velocities are computed in the following way. First, the P- and S-wave velocities are measured with the "first break" technique on the "room dry" rock samples and the corresponding rock density measured independently. These data are converted into bulk and shear moduli which are identified with the drained bulk modulus $K^{(dr)}$ and shear modulus μ, as mentioned above. Then, assuming $K^{(fl)}$ = 2.25 GPa (saturating fluis is water) and $K^{(gr)}$ = 37 GPa (quartz grain) for sandstones, $K^{(gr)}$ = 73.3 GPa (calcite grain) for limestones and $K^{(gr)}$ = 94.9 GPa (dolomite grain) for dolomites the undrained bulk modulus is computed using Equations (7, 8) and (9), and the undrained P- and S-wave velocities using Equation (10) with independently measured density of the fluid-saturated rock sample.

TABLE 1

Average values of the density, the bulk and shear moduli of the main mineral constituents of the sedimentary rocks (Bass, 1995; Zinszner and Pellerin, 2007)

Mineral	Density (kg/m^3)	Bulk modulus (GPa)	Shear modulus (GPa)
Quartz	2 650	37	45
Calcite	2 710	70	30
Dolomite	2 870	80	50
Siderite	3 960	120	50
Clay (average)	2 750	25	9

The rough correlation observed in Figure 1, especially for the P-wave velocity (correlation coefficient ≈ 0.83), could lead to question the applicability of the poroelastic theory for ultrasonic experiments in the laboratory. In fact, it has been demonstrated by Rasolofosaon *et al*. (2008) in carbonates that the agreement between experiment and theory can be greatly improved by carefully adapting the experimental procedures.

This is illustrated in the next sections on various types of rocks (*i.e*. sandstones, dolomites, limestones, and dolomitic limestones).

2.2 Experimental Procedure and Corroboration of the Theory

In this part, we briefly describe the alternative experimental set-up and procedure and illustrate three types of experimental verifications of Biot-Gassmann equations on rock samples.

2.2.1 Experimental Set-Up and Procedure

The experimental set-up is that used by Rasolofosaon and Zinszner (2004a) and shown in Figure 2. The measurement cell corresponds to a standard device for measurement under

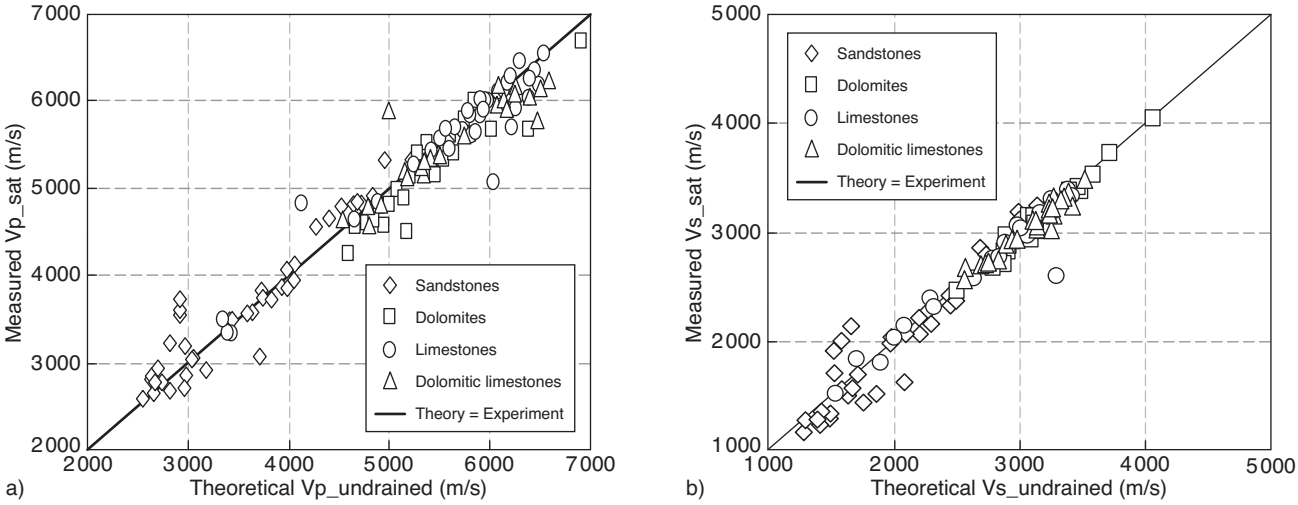

Figure 1

Measured first-break velocities (a: *P*-wave, b: *S*-wave) as functions of the theoretically predicted velocities using poroelastic equations on water-saturated rocks (312 samples of sandstones, dolomites, limestones, and dolomitic limestones from the open literature).

confining pressure. The rock sample, 40 mm in diameter and 40 to 80 mm in length, is placed in a Viton sheath which partly covers the two measurement heads each containing an ultrasonic transducer. In our experiment, we use double *P* and *S* transducers (two half-moon ceramics) yielding very high quality signals.

Once equipped, the cell is filled with oil which when pressurized allows a maximum confining pressure P_c of 70 MPa. A pump controls the pore pressure P_p inside the sample. The condition $P_p < P_c$ must always be observed in order to preserve the Viton sheath and to avoid to put the rock in tension. The cell allows to measure *P*- and *S*-waves ultrasonic velocities (central frequency around 500 kHz) under controlled pore and confining pressures.

Regarding the experimental procedures, we emphasized the fluid substitution technique and the velocity measurements. During the various fluid substitutions, the rock sample is not moved and stays in the measurement cell. Measurements are always performed under 100% saturation with the considered fluid or fluid mixtures. This allows to avoid any modification of the acoustic coupling between the rock sample and the measurement device and, as a consequence, to achieve more accurate and more comparable measurements. We use various types of saturating fluids (*e.g.*, water, ethanol, kerosene, soltrol... and mixture of liquids) of contrasted physical properties as illustrated by Table 2 (Rasolofosaon and Zinszner, 2004a).

Any chemical reaction with the rock must be avoided. As a consequence, the choice of the saturating liquid mainly depends on the presence of clay in the rock sample. For limestones and clean sandstones, one can easily use liquids

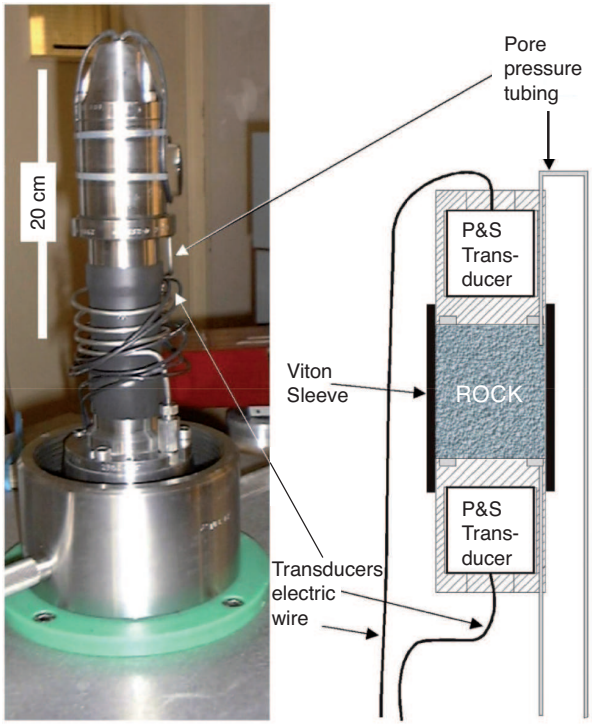

Figure 2

Photograph and diagram of the cell for acoustic measurement under controlled pore and confining pressures.

with bulk modulus $K^{(fl)}$ in the range 0.7 GPa (pentane) to 3.2 GPa (ethylene glycol) and even 4.8 GPa (glycerol). In clayey sandstones it is safer to use brine or hydrocarbons, and the range of possible values for $K^{(fl)}$ is narrower (maximum

TABLE 2

The saturating fluids used in this work and their physical properties, namely from left to right bulk modulus (in GPa), density (in kg/m^3) and viscosity (in 10^{-3} Pa.s)

Liquid	Bulk modulus (GPa)	Density (kg/m^3)	Viscosity (10^{-3} Pa.s)
Pentane	0.72	625	0.25
Heptane	0.88	683	0.40
Hexane	0.90	675	0.30
Ethanol	1.12	795	1.20
Soltrol	1.16	752	1.50
Kerosene	1.40	804	
Bromoform 75% ethanol	1.55	1 720	
Trichlorethylene	1.73	1 461	
Albelf	1.90	863	170
Polyal	1.92	845	1 100
Ethanol 40% ethy. glyc.	2.11	957	5
Water	2.25	1 000	1
Brine 25 g/L	2.30	1 020	1
Bromoform	2.45	2 800	
Aniline	2.90	1 019	5
Ethylene glycol	3.23	1 112	19
Glycerol	4.80	1 263	1 500

$K^{(fl)}$ corresponding to brine is 2.4 GPa) but still enough to accurately test the theory.

Regarding velocity measurements, in order to avoid errors related to "path dispersion" due to heterogeneities of dimension non-negligible compared to the wavelength, especially in limestones (Cadoret, 1993; Cadoret *et al*., 1995; Rasolofosaon and Zinszner, 2008), we performed phase velocity measurements using the spectral ratio technique (*e.g*., Pouet and Rasolofosaon, 1993). Compared to the simplest and also the most used technique, namely the first break technique, the phase velocity technique allows to limit the effect of the rock heterogeneity on the ultrasonic measurements, as demonstrated by Rasolofosaon and Zinszner (2008) in limestones.

In the next sub-sections, we illustrate three types of experimental verifications of the poroelastic equations on rock samples.

2.2.2 Relation between Bulk Moduli of Rock and Fluid

The first type of experimental verification, illustrated by Figure 3, is about the link between the undrained moduli (bulk moduli in black circles and shear moduli in grey triangles) of the saturated rock and the bulk modulus of the saturating fluids reported in Table 1. The considered rock is Estaillades limestone, a highly porous rock (ϕ = 30%) with an average permeability (k = 180 millidarcy). This bioclastic limestone

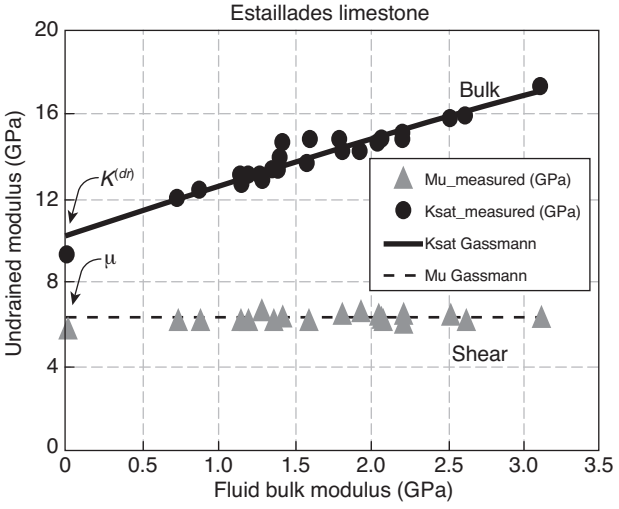

Figure 3

Experimental undrained bulk modulus (black circles) and shear modulus (grey triangles) as functions of the bulk modulus of the saturating fluid. Poroelastic theoretical predictions are in solid line for bulk modulus and in dashed line for shear modulus.

has a bimodal porous network with abundant intergranular porosity and large microporosity contained in the bioclasts. We note the good agreement between experimental data and the theoretical predictions (solid line for the bulk modulus and dashed line for the shear modulus). For the model, we took for the drained bulk modulus $K^{(dr)}$ and shear modulus μ the limit of the measured bulk and shear modulus of the rock for vanishing fluid modulus $K^{(fl)}$ instead of measuring the wave moduli of the dry rock, the "room dry" condition being not well controllable.

We also note in Figure 3 a nearly linear dependence of the undrained bulk modulus $K^{(u)}$ the fluid-saturated rock with the bulk modulus $K^{(fl)}$ of the saturating fluid. This can straightforwardly be deduced from the poroelastic equations. As a matter of fact if one assumes that the solid grain is much less compressible than the saturating fluid:

$$K^{(fl)} << K^{(gr)} \tag{12}$$

which is quite a reasonable assumption in most practical situations in Rock acoustics (compare $K^{(gr)}$ values in *Tab. 1* with $K^{(fl)}$ values in *Tab. 2*). Under this assumption, Equation (9) becomes:

$$M \approx K^{(fl)}/\phi \tag{13}$$

Equation (13) reported in Equation (7) gives:

$$K^{(u)} \approx K^{(dr)} + \frac{\alpha^2}{\phi} K^{(fl)} \tag{14}$$

The simplified Equation (14) means that the undrained bulk modulus $K^{(u)}$ is approximately a linear function of the bulk

modulus $K^{(fl)}$ of the saturating fluid, which is clearly shown in Figure 3 and commonly observed in all the rock samples that we studied.

2.2.3 Shear Modulus Independent of the Saturating Fluid

As pointed out in the first section, one of the most important results of the poroelastic theory is the independence of the shear modulus of the rock with respect to the properties of the saturating fluid, more specifically the viscosity. This is clearly illustrated by Figure 4 on sintered quartz (left) and Fontainebleau sandstone (right). In sintered quartz the viscosity of the saturating fluid clearly has no measurable influence on the shear modulus. Only the level of differential pressure P_{diff}, the difference between the confining pressure P_c and the pore pressure P_p, modifies the shear modulus of the rock. As widely known, an increase of P_{diff} induces a stiffening of the rock (increase of bulk and shear moduli) by closing the cracks and compliant pores (Mavko *et al*., 1998). The effect is weak on sintered quartz because sintering tends to eliminate most of the cracks. In Fontainebleau sandstones, and in all the rocks that we analyzed, the independence of the shear modulus of the rock with respect to the viscosity of the saturating fluid is observed for sufficiently large differential pressure P_{diff} (typically > 5 MPa), that is to say when a sufficient number of compliant pores is closed.

2.2.4 Verification on the Bulk Modulus of Grain Constituent

Up to now, the bulk modulus of the grain constituent $K^{(gr)}$ was inferred from the knowledge of the mineralogical composition of the rock sample.

The bulk modulus $K^{(gr)}$ of the grain constituent, together with the fluid bulk modulus $K^{(fl)}$, the drained bulk modulus $K^{(dr)}$ and the porosity φ of the rock are the basic input parameters of the Biot-Gassmann Equations (8) and (9). Although not commonly done, one can compute $K^{(gr)}$ from the measured values of the undrained bulk modulus $K^{(u)}$, the drained bulk modulus $K^{(dr)}$, the fluid bulk modulus $K^{(fl)}$ and the porosity ϕ appearing in Equations (7, 8) and (9), using the relation:

$$K^{(gr)} = \frac{-b - \sqrt{\Delta}}{2a} \text{ and } \begin{cases} a = \phi(K^{(u)} - K^{(dr)}) - K^{(fl)} \\ b = K^{(fl)}\left[K^{(dr)}\left(1+\phi\right) + K^{(u)}\left(1-\phi\right)\right] \\ c = -K^{(u)}K^{(dr)}K^{(fl)} \\ \Delta = b^2 - 4ac \end{cases} \quad (15)$$

This computation is useful for checking experimentally the validity of Biot-Gassmann equations because the bulk modulus $K^{(dr)}$ of the main mineral constituents of the sedimentary rocks are known *(see Tab. 1)*. These theoretical values can be compared to the values obtained from the experiments.

Note that the value of $K^{(gr)}$ obtained by Equation (15) is very sensitive to small variations of the input parameters.

Without going into a systematic analysis, we can give a simple numerical example. Figure 5 considers a typical non-clayey sandstone and a typical limestone, both water-saturated and with porosity equal to 0.2. The drained bulk modulus $K^{(dr)}$ is kept constant and equal to 17 GPa for the sandstone and 19 GPa for the limestone. One immediately observes the large error induced on the estimation of bulk modulus of the grain constituent $K^{(gr)}$ by a variation of less than 10% of the

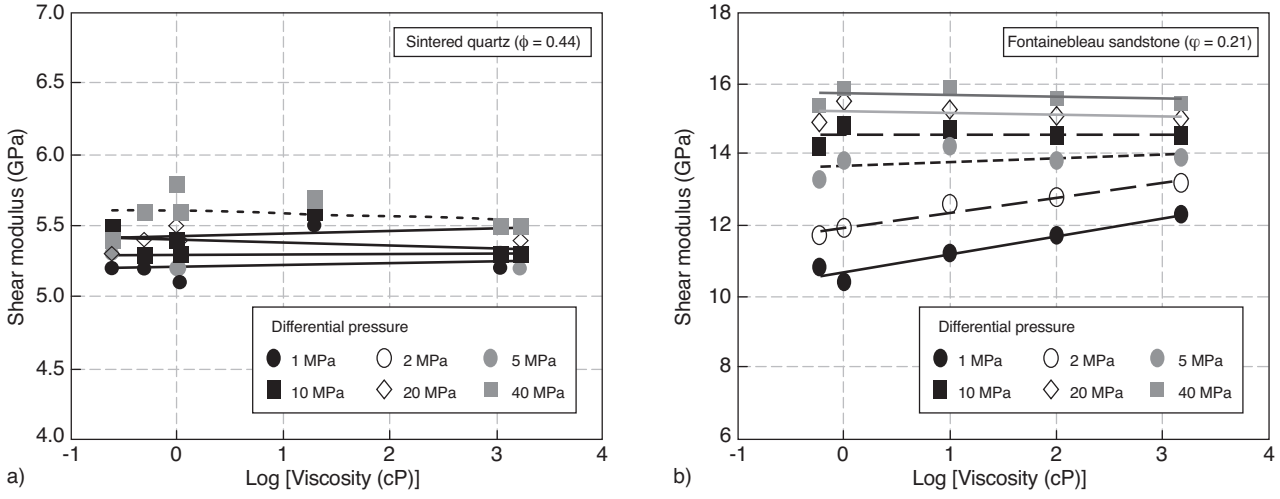

Figure 4

Shear modulus (in GPa) of the saturated medium as function of the logarithm of the viscosity of the saturating fluid (in centipoise) under 6 fixed levels of differential pressures (1, 2, 5, 10, 20 and 40 MPa). a) Case of sintered quartz, and b) case of Fontainebleau sandstone. The different lines correspond to linear fits on the corresponding data.

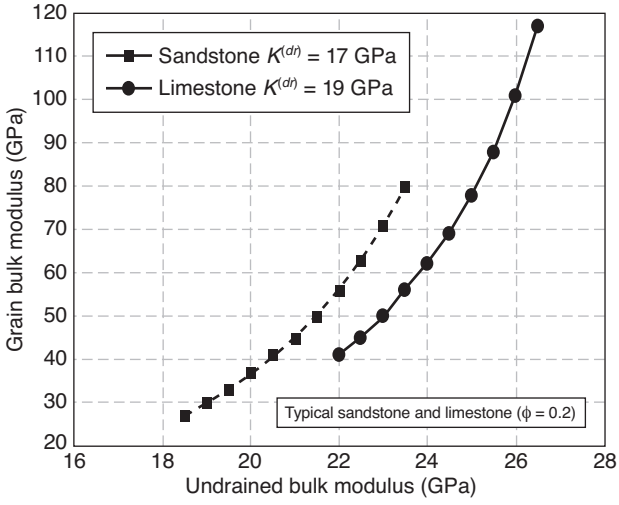

Figure 5

Variations in the evaluation of the bulk modulus $K^{(gr)}$ of the grain constituent by Equation (15) as a function of variations on the value of the exact undrained bulk modulus $K^{(u)}$ for typical sandstone (black squares) and limestone (black circles).

value of the undrained bulk modulus $K^{(u)}$ of the rock about an average value. The induced error is larger than 45% for the sandstone and reaches 100% for the limestone. Such a result is very encouraging for our approach of validation of the proposed experimental procedure. For instance, this will allow to favorably interpret deviations as large as 10% to 20% between the experimentally determined $K^{(gr)}$ and the corresponding theoretical value read in Table 1.

The two next tables allows a quality control of the proposed experimental procedure using the experimental estimation of $K^{(gr)}$. Table 1 compares estimations of $K^{(gr)}$ deduced from ultrasonic velocity measurements using three techniques on water-saturated Estaillades limestone under four different confining pressures, namely 1, 2, 5 and 10 MPa. Three measurement techniques are the most common technique, name the first break technique, the correlation technique and the spectral ratio technique, for phase velocity measurement. In the correlation technique, the signal to be analyzed is compared, by time correlation, with a reference signal of known transit time.

We notice that the first break technique and the correlation technique systematically overestimate $K^{(gr)}$. Only, the phase velocity measured by the spectral ratio technique gives a correct estimation the bulk modulus of the grain constituent.

The overestimation of $K^{(gr)}$ by the correlation technique and the first break technique is simply due to the overestimation of the undrained bulk moduli $K^{(u)}$ of the fluid-saturated rock, resulting themselves from the overestimation of the *P*-wave velocity. This is why we think that the disagreements between experimental results and the predictions of Biot-Gassmann theory reported in the literature, at least in the laboratory, are mainly due to unsuitable experimental techniques, especially with respect to velocity measurements. If phase velocity are correctly measured the experimental results are clearly consistent with the poroelastic theory, as illustrated also by Table 4 in Fontainebleau sandstone.

TABLE 3

Bulk modulus $K^{(gr)}$ (in GPa) of the grain constituent deduced from ultrasonic velocity measurements in the laboratory on water saturated Estaillades limestone with calcite as a major grain constituent under 4 different differential pressures, namely 1, 2, 5 and 10 MPa. Three velocity measurements techniques, namely first break peaking (the most commonly used), correlation technique, and phase spectrum analysis, are compared. Only, the last technique gives the correct value (70 GPa for Calcite) of the bulk modulus K_{grain} of the grain constituent using the poroelastic equations

Measurement technique	P_{diff} = 1 MPa	P_{diff} = 2 MPa	P_{diff} = 5 MPa	P_{diff} = 10 MPa
First break	115	116	116	104
Correlation		193	135	128
Phase	79	89	64	69

TABLE 4

Bulk modulus (in GPa) of the grain constituent deduced from ultrasonic velocity measurements in the laboratory on Fontainebleau sandstone with quartz as the only grain constituent (correct value of $K^{(gr)}$ for quartz is 37 GPa). The rock sample is saturated by 8 different fluids and 5 different confining pressures are considered, namely 2, 5, 10, 20 and 40 MPa

P_{diff}	Brine	Polyal	Kerosene	Heptane	Pentane	Methanol	Ethylene glycol	Glycerol
2 MPa	38	39	31	28	33	31	35	36
5 MPa	37	36	33	33	33	30	34	36
10 MPa	32	33	32	32	32	32	33	36
20 MPa	33	35	34	35	35	33	35	35
40 MPa		37	35	35	34	34	35	36

In contrast with the previous experiment here, eight different saturating fluids were used, and five different confining pressures are imposed, namely 2, 5, 10 and 20 MPa. Here again, we note that all the experimentally deduced grain-constituent stiffness $K^{(gr)}$ using Equation (15) are surprisingly not very different from the bulk modulus of quartz, namely 37 GPa *(see Tab. 1)* the only constituent of this rock.

The new experimental procedures have been checked on a database containing 76 rock samples of various types. We chose the following groups of rocks:

– Fontainebleau sandstone (different porosities ϕ = 0.2, 0.14 and 0.07), a well-sorted very clean (nearly 99.8% quartz)

sandstone composed of sub-spherical grains of quartz of roughly 250 μm diameter with a simple porous network (*e.g.*, Bourbié *et al*., 1987);

– Weakly (Vosges) and moderately (Meule) clayey sandstones. Only a few number of samples were available. Numerous other samples were rejected because the measurement technique was slightly different from that imposed in the present study. However, a large buch of acceptable measurements were available on the remaining samples. These sandstone samples exhibited porosities around 0.20 to 0.25 (5 samples);
– a large group of samples (23) of weakly to moderately porous limestones ($\phi < 0.3$). The main interest of such a collection of samples is to allow a statistical analysis on mono-mineral (calcite) carbonates, sometimes considered to be not really appropriate for the validation of Biot-Gassmann theory;
– about fifteen very porous ($\phi > 0.3$) limestones, which often cause major experimental in the correct recording of *S*-waves.

In spite of the diversity of the new selection of rock samples, Biot-Gassmann equations are clearly much better corroborated (correlation coefficient > 0.98), as illustrated by Figure 6, to be compared with Figure 1 with the same type of plot.

3 EXPERIMENTAL RESULTS ON PRESSURE DEPENDENCE

This section deals with the pressure dependence of the velocities. First, we experimentally verify that velocities essentially depends on the differential pressure $P_{diff} = P_c - P_p$ (the difference between the confining pressure P_c and the pore-pressure P_p), and not in an independent way on P_c and on P_p. Then, we illustrate the relevancy of Hertz-type model of pressure dependence of the velocities. Finally, we quantify and discuss Hertz coefficients in outcrop and core samples.

3.1 Importance of the Differential Pressure

The simplest way to unambiguously show the relevancy of the differential pressure $P_{diff} = P_c - P_p$ for the pressure dependence of the velocities is to measure the *P*- and *S*-wave velocities under different states of pore pressure P_p and confining pressure P_c and to check the pressure pairs (P_c, P_p) that keep the considered velocity unchanged. Our experimental set-up shown in Figure 2 allowing to measure the ultrasonic velocities under controlled pore and confining pressures, we investigated on each rock sample the various pressure states (diamond points) plotted in Figure 7. Note that the condition $P_p < P_c$ is always observed.

At each pressure state, we measured both *P*- and *S*-wave velocities. The pressure grid was dense enough to allow plotting iso-velocity maps such as those illustrated by Figure 8 in Meule sandstone saturated with Albelf.

This is just an example but is typical of all the rocks that we have analyzed. One clearly sees that the iso-velocity lines are practically parallel to the first diagonal $P_c = P_p$, which means that *P*-wave *(Fig. 8a)* and *S*-wave *(Fig. 8b)* velocities only depend on the differential pressure $P_{diff} = P_c - P_p$, and not in an independent way on P_c and on P_p. The link with the

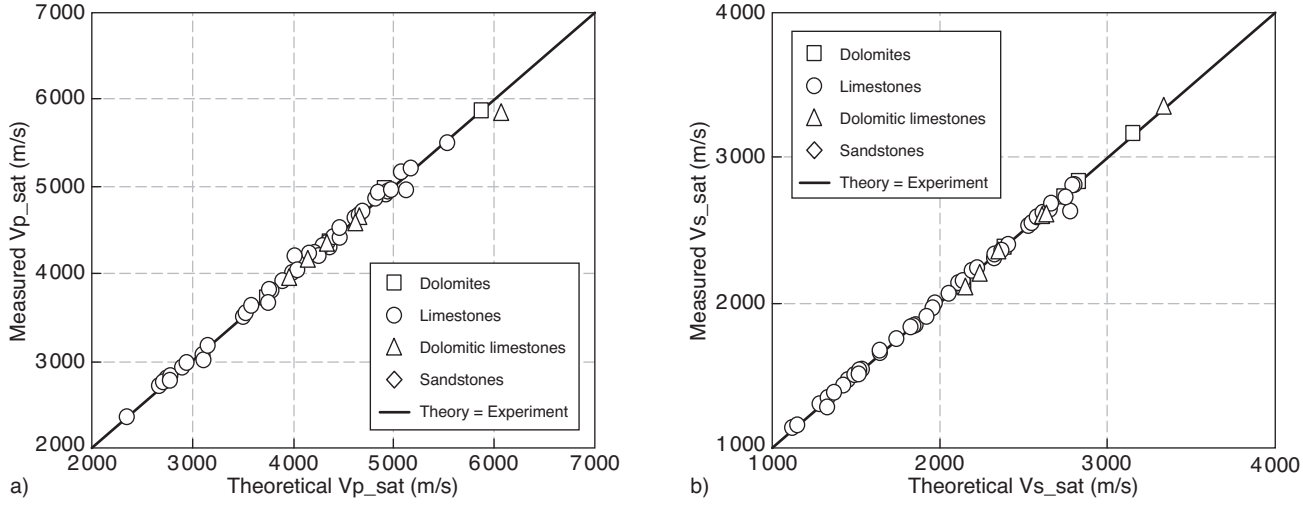

Figure 6

Measured phase velocities (a) *P*-wave. b) *S*-wave) as functions of the theoretically predicted velocities using poroelastic equations on water-saturated rocks using the fluid-substitution and phase velocity techniques described in the text (76 samples of sandstones, dolomites, limestones, and dolomitic limestones). Same convention plot as Figure 1.

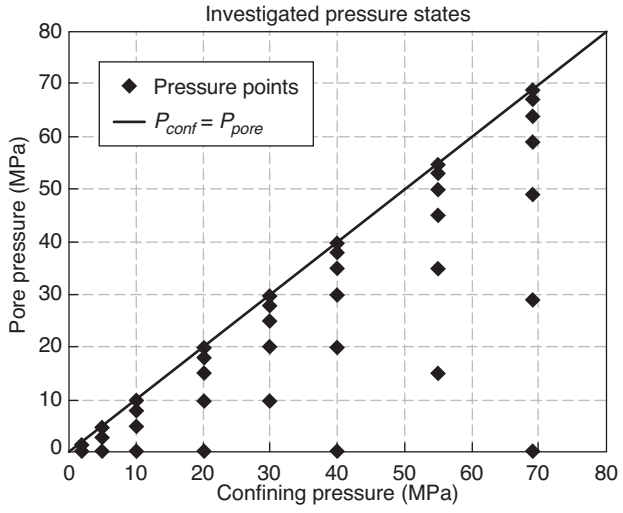

Figure 7

Investigated pressure states (black diamonds) plotted in the plane of pore pressure P_p and confining pressure P_c.

differential pressure and the effective pressure concept introduced in Equation (4) and in the corresponding comments is the following. In fact, the effective pressure (we use pressure instead of stress for simplicity of the explanation) is not an absolute concept but is relative to the effective physical property under consideration. More precisely, the effective pressure $P_{eff}^{(\Pi)} = P_c - n^{(\Pi)}P_p$, relative to a physical property Π, is a linear combination $P_c - n^{(\Pi)}P_p$ of the confining pressure P_c and of the pore pressure P_p that leaves the physical property Π unchanged, in spite of the separate and simultaneous change of P_c and P_p. The constant $n^{(\Pi)}$ is called the effective stress coefficient relative to the physical property Π. For the bulk volumetric strain $n^{(\Pi)}$ is equal to Biot's poroelastic coefficient $\alpha = 1 - \frac{K^{(dr)}}{K^{(gr)}}$ (*e.g.*, Nur and Byerlee, 1971; Robin, 1973), which is the case in Equation (4). In contrast, for the porosity and for the drained bulk modulus $n^{(\Pi)}$ is equal to 1 in idealized model (*e.g.*, Zimmermann, 1991; Gurevich, 2004). In other words, for these physical properties the effective pressure is equal to the differential pressure. Our experimental data on various rock samples, not all shown here, show that $n^{(\Pi)}$ relative to the elastic velocities of the fluid-saturated rocks does not differ much from 1.

In detail, this is not exactly verified for the case of high pore pressure P_p (that is to say close to the diagonal $P_c = P_p$) and small level of confining pressure P_c, especially for the *P*-wave. We give an explanation of this phenomenon in the comments of the next figures.

Figure 9 also illustrates in a different way the importance of the differential pressure P_{diff} in the pressure dependence of the velocities. We plotted the experimental *P*-wave velocity *(Fig. 9a)* and *S*-wave velocity *(Fig. 9b)* in water-saturated Vosges sandstone as functions of the confining pressure P_c, for five levels of the differential pressure, namely P_{diff} = 1, 2, 5, 10 and 20 MPa. Experimental data are plotted in dashed lines with different symbols corresponding to different levels of P_{diff}. The main result, totally in agreement with Figure 8, is the relative constancy of the velocities with respect to confining pressure for fixed differential pressure P_{diff}. This is particularly well verified for *S*-wave velocity (right figure) and to a lower extent for the *P*-wave velocity.

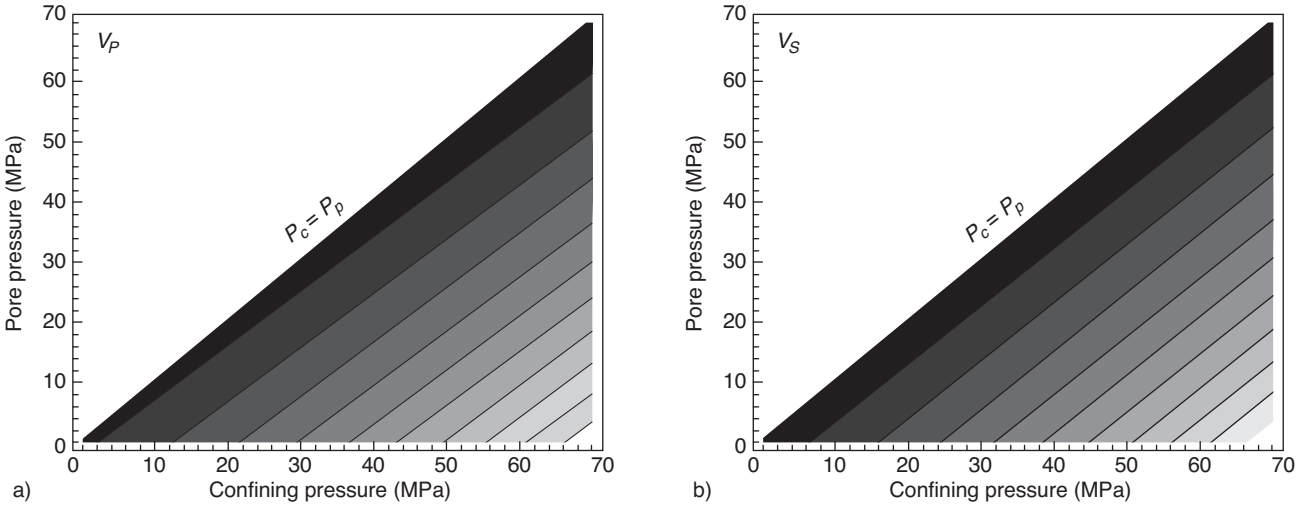

Figure 8

Experimental iso-velocity maps of the *P*-wave a), and of the *S*-wave b), in the plane of confining pressure P_c and pore pressure P_p. Case of Meule sandstone saturated with Albelf.

The central influence of the differential pressure P_{diff} on the velocities is classically explained in the following way (Bourbié *et al*., 1987; Mavko *et al*., 1998). An increase of the confining pressure P_c tends to close the mechanical defects (*i.e*., grain contacts, micro-cracks, micro-fractures...) contained in the rock, thus to stiffen the rock, and as a consequence to increase the seismic velocities, without greatly affecting its porosity. In contrast, the pore pressure P_p in the saturating fluid tend to open the pores, especially the flat compliant pores (constituting the mechanical defects). This is the major effect. The effect of the pore pressure P_p on the *S*-wave velocities is nearly exactly equilibrated by the effect of the confining pressure P_c *(Fig. 9b)*. This does not hold exactly for the *P*-wave velocities *(Fig. 9a)*. We observe a moderate increase of *P*-wave velocity with confining pressure for fixed differential pressure, the smaller P_{diff} the larger the phenomenon.

This can be clearly explained by an additional effect, not classically taken into account, namely the dependence of the bulk modulus of the saturating fluid (brine in this case) with the pore pressure P_p. In effect, in moderately pressure-dependent porous media Biot-Gassmann equations still roughly holds, but all the coefficients now depend on the pressure level. First of all, the pressure dependence of the grain constituent modulus is negligible compared to that induced by other constituents (*i.e*., fluid content, pores...) (Guyer and Johnson, 1999; Johnson and Rasolofosaon, 1996; Rasolofosaon and Yin, 1996). Beside the major role of the compliant features (*e.g*., grain-to-grain contacts, low-aspect-ratio cracks, joints...), omnipresent in rocks, in the pressure dependence of the velocities, the contribution of the nonlinearity of the saturating fluid must not be neglected.

Figure 10 shows the increase of the Bulk modulus $K^{(fl)}$ of five different saturating liquids, namely Water, Ethylene glycol, Soltro, Methanol and Heptane, as function of the pore pressure P_p. This is known as the nonlinear elasticity of the liquids (Anderson, 1971; Daridon *et al*., 1999; Plantier *et al*., 2002; Tamura *et al*., 1994). If this effect is neglected, the undrained bulk modulus $K^{(u)}$ of the liquid-saturated rock should not depend on the pore pressure P_p for fixed differential pressure P_{diff}, which is clearly contradicted by the experimental result on *P*-waves *(Fig. 9a)*. Furthermore, the observed increase of $K^{(u)}$ with the confining pressure P_c, or equivalently with decreasing pore pressure P_p; for fixed differential pressure P_{diff} can be perfectly predicted by a taking into account not only the fluid substitution and the dependence with P_{diff} of the velocities, summarized by Hertz-type Equation (11), but also the dependence of the fluid bulk modulus $K^{(fl)}$ on the pore pressure P_p, illustrated by Figure 10 and due to the nonlinear elasticity of the saturating liquid. This is well illustrated by Figure 9, where the theoretical predictions taking into account the nonlinearity of the saturating liquid, plotted in solid lines, are in a reasonable agreement with the experimental results in water-saturated Vosges sandstone. The model correctly predicts a slight increase of the *P*-wave velocity with confining pressure P_c, for fixed differential pressure P_{diff}. In effect, the pore pressure P_p simultaneaously increases with the confining pressure P_c to ensure a constant differential pressure P_{diff}. As a consequence the pore pressure increase induces an increase of the bulk modulus $K^{(fl)}$ of the saturating fluid, as shown by Figure 10, which results in the increases of the undrained bulk modulus $K^{(u)}$ and of the *P*-wave velocity, according to Equations (10) and (14).

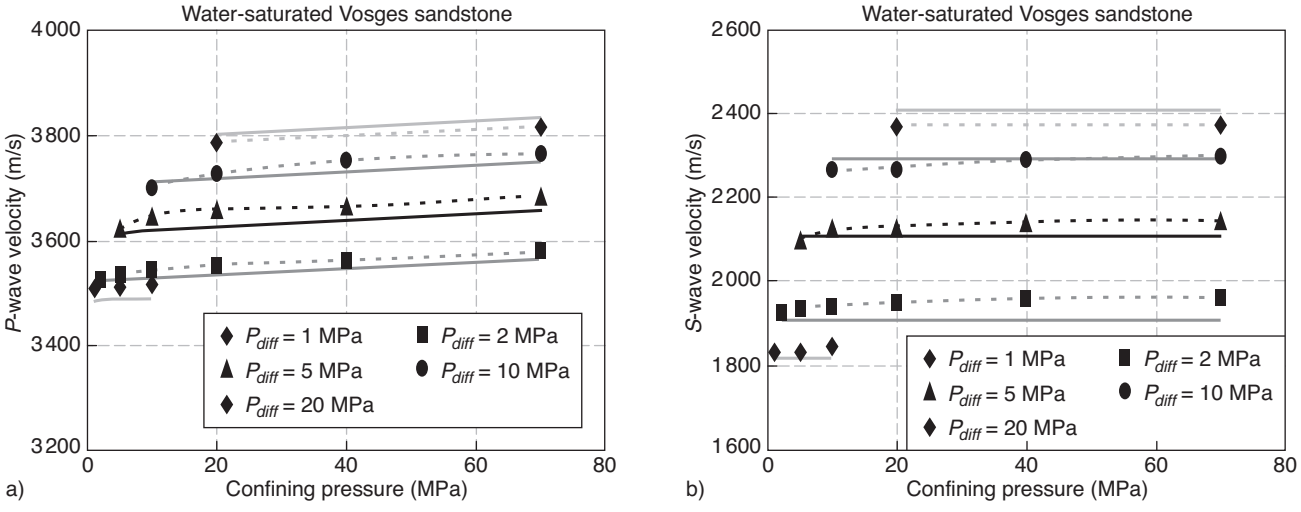

Figure 9

Experimental *P*-wave velocity a) and *S*-wave velocity b) as functions of the confining pressure, for five levels of the differential pressure P_{diff}. Case of water-saturated Vosges sandstone.

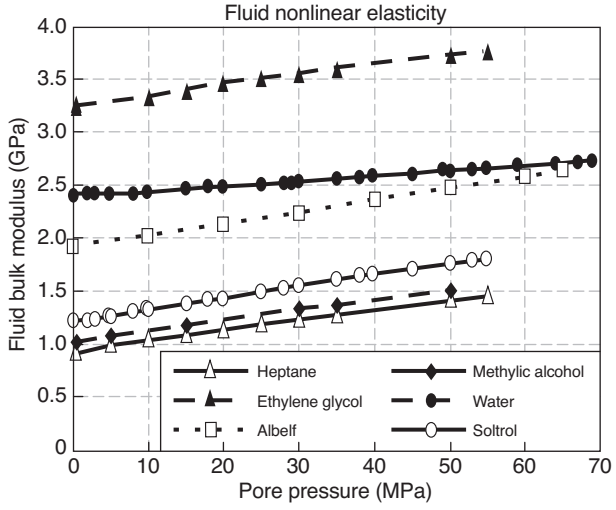

Figure 10

Bulk modulus $K^{(fl)}$ of the saturating fluid as a function of the pore pressure P_p for some of the liquids of Table 2.

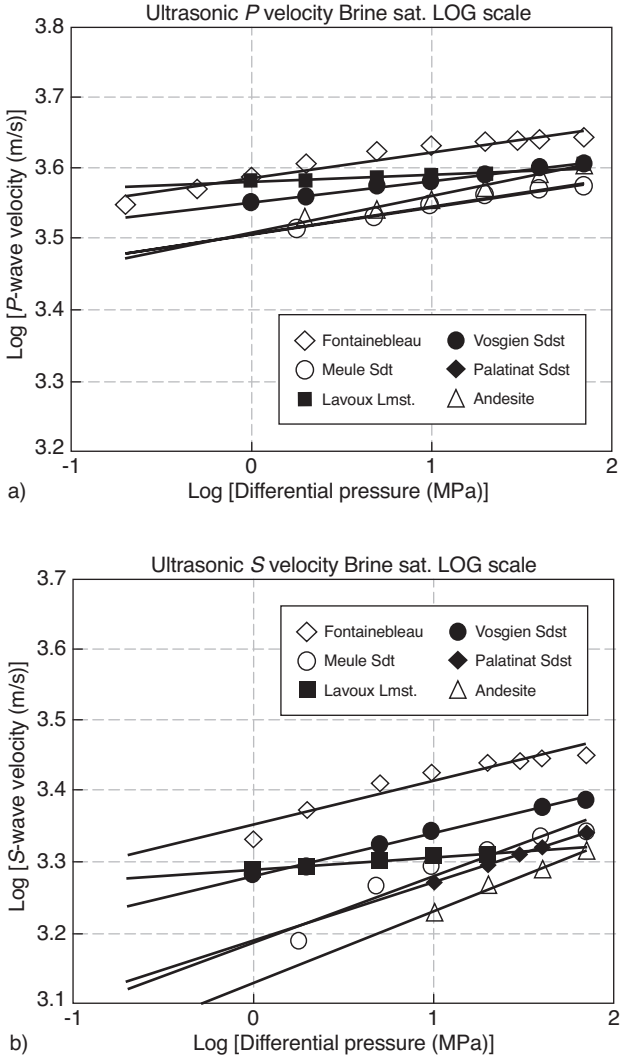

Figure 11

Ultrasonic *P*-wave velocity a) and *S*-wave velocity b) as functions of the differential pressure in Log-Log scale in five rock samples. Solid lines are linear regression curves.

This does not affect the *S*-wave velocity because the shear modulus is not affected by the presence of the fluid, as extensively demonstrated in a previous section and illustrated by Figures 3 and 4.

3.2 Relevancy of Hertz-Type Model

Figure 11 illustrates the relevancy of a power law for the dependence of the velocities with the differential pressure P_{diff}. Ultrasonic *P*-wave velocity *(Fig. 11a)* and *S*-wave velocity *(Fig. 11b)* are plotted as functions of the differential pressure in Log-Log scale. Five rock samples are considered and can be considered as representative of the rock samples that we analyzed. The data points are represented by various symbols and the solid lines are the corresponding linear regression curves.

The agreement between a theoretical power law (linear regression in Log-Log scale) and the experiment results is reasonable enough to avoid the further refining of the pressure-dependent model.

3.3 Hertz Coefficients in Rocks

3.3.1 General Remarks

Figure 11 not only illustrates the relevancy of the Hertz-type model for describing the pressure dependence of the velocities, but also summarizes the main trends of rock behaviour:

– Lavoux limestone illustrates the clear trend of limestones from outcrops to exhibit no or weak dependence of the velocities (*P* and *S*) with the differential pressure;

– the sandstones, except Fontainebleau sandstone, follow a power law in the investigated pressure interval. However, one can notice some trend of stabilization for high differential pressure (larger than 60-70 MPa). The slopes of all the linear regression lines are not very different from each other with Hertz exponent h_P of the order of 50×10^{-3} for *P*-wave. Hertz exponent h_S for *S*-wave is substantially larger, with values around 80×10^{-3}.

For this study, we collected numerous data from the literature and data from our laboratory at IFP Energies nouvelles. Neither the measurement accuracy nor the pressure interval for the computation of Hertz exponents (between 5 et 40 MPa in most rock samples) were the same for all these

data. However, the great number of measurements statistically makes up for these weaknesses. The results are synthesized for outcrop and core samples as histograms in Figures 12 and 13, respectively in sandstones and in limestones. The first result is the difference between core samples and outcrop samples. Core samples statistically exhibiting larger Hertz exponents than outcrop samples will be studied separately.

3.3.2 Outcrop Samples

The observations made on the rock samples of Figure 11 are confirmed by the histograms of Figures 12 and 13. Velocities in Limestones are weakly sensitive to pressure (h_P and h_S of the order of 15×10^{-3} and 25×10^{-3} respectively). For sandstones Hertz exponents are notably larger, with modal values of the order of 40×10^{-3} for h_P, and 60×10^{-3} for h_S.

If one tries to clarify the link between Hertz exponent and some petrophysical parameters, the results are not really convincing. For instance, the link between porosity and Hertz exponent is fuzzy, as illustrated by Figure 14. Hertz exponents for outcrop samples (black symbols) and in core samples (empty symbols) are plotted as functions of the porosity in sandstone *(Fig. 14a)* and in limestones *(Fig. 14b)*. *P*-wave

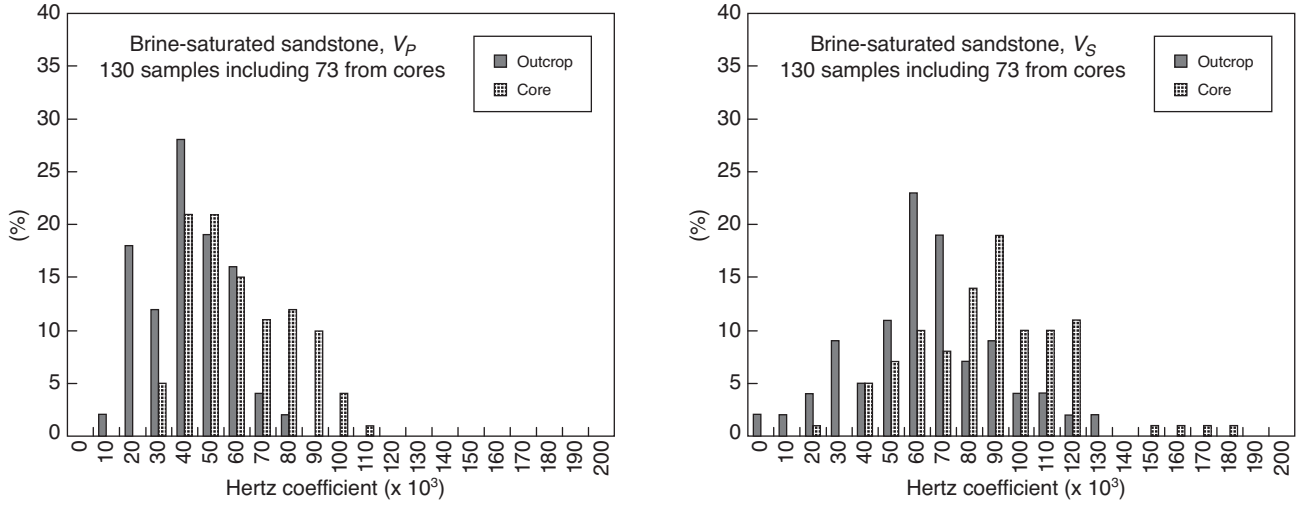

Figure 12

Histograms of Hertz exponents for *P*-wave (left) and *S*-wave (right) in outcrop and reservoir samples of brine-saturated sandstones.

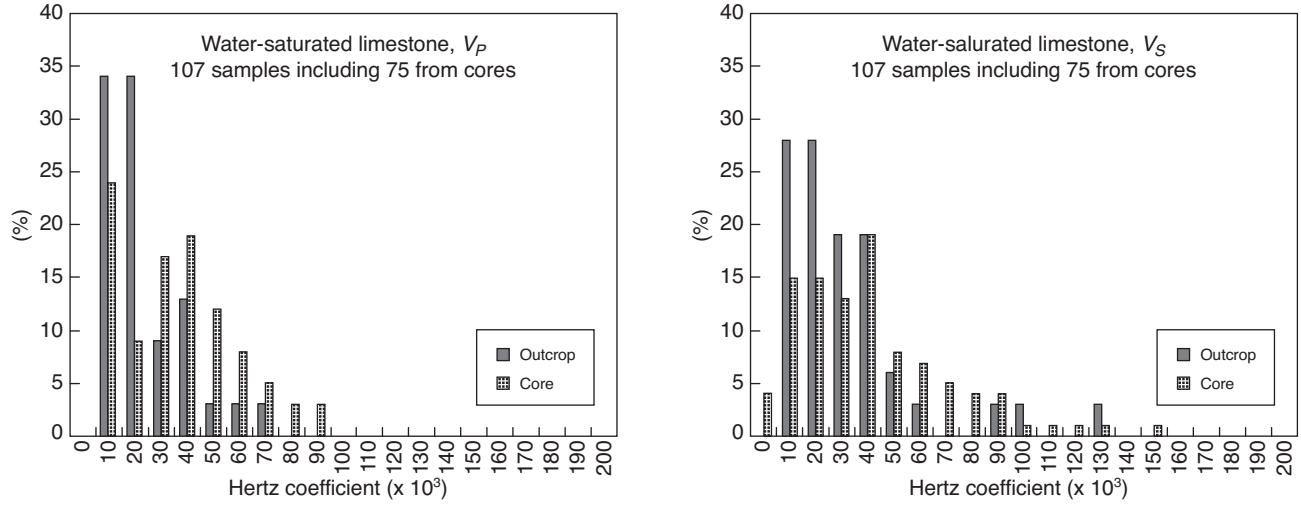

Figure 13

Histograms of Hertz exponents for *P*-wave (left) and *S*-wave (right) in outcrop and reservoir samples of brine-saturated limestones.

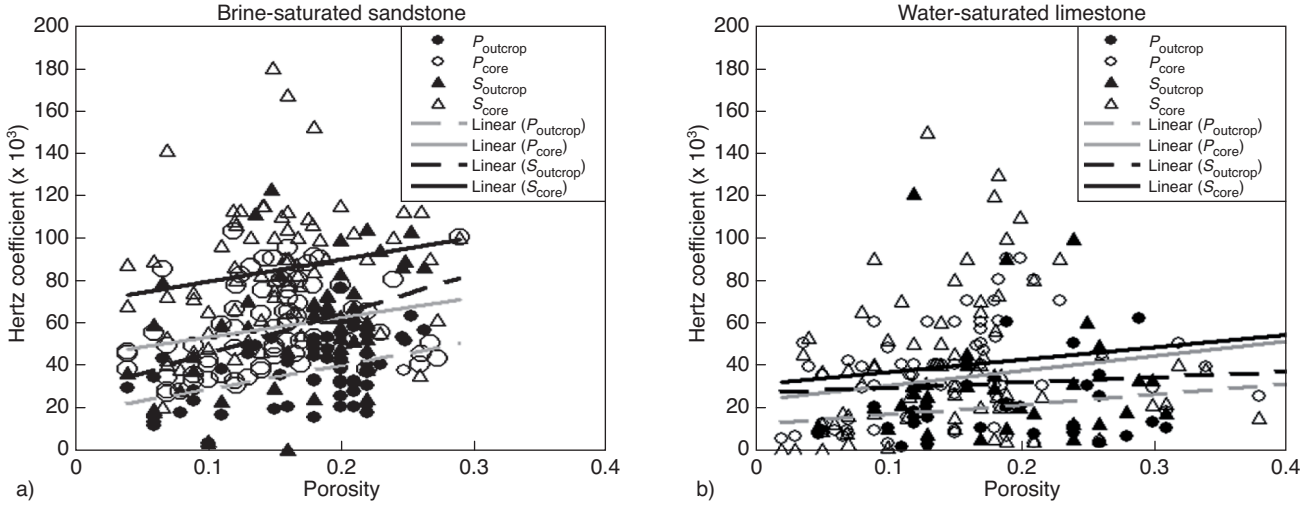

Figure 14

Hertz exponents for *P*-wave (circles) and for *S*-wave (triangles) in outcrop samples (black symbols) and in core samples (empty symbols) as functions of the porosity in brine-saturated sandstone a) and in water-saturated limestone b). The straight lines are linear fit on the experimental data.

corresponds to circles and *S*-wave to triangles. The straight lines are linear fit on the experimental data. Solid lines correspond to core samples and dashed lines to outcrop samples. Grey lines correspond to *P*-wave and black lines to *S*-wave. Sandstones exhibit some correlation, as shown by the small slope of the linear fit curves both in outcrop and core samples. Porosity does not seem to be a key parameter. In effect, if one classifies the porosity in two types, namely from one side the sub-spherical stiff pores, representing the major part of the porosity in reservoir rocks, and from the other side the thin compliant pores (*e.g.*, grain-to-grain contacts, low-aspect-ratio cracks, joints...). The latter type of pores, although representing a minute part of total porosity, is the main cause of the dependence of the velocities with the differential pressure (Walsh et Brace, 1966). Practically, these thin compliant pores do not contribute to the total porosity of reservoir rocks (obviously the situation is different in the case of compact rocks). As a consequence, it is not surprising that there is a lack of evident link between the total porosity and Hertz exponent.

The micas seem to play a major role in some sandstones. Even a small number of very small crystals can induce strong dependence of the velocities with differential pressure, or equivalently corresponding large Hertz exponents. Our observations were mainly made on core samples. It would be interesting to study on outcrop samples the actual consequences of the processes of alteration and stress relaxation on the mica effect.

3.3.3 Core Samples – Stress-Relaxation Effects

During the recovery of the core samples the rock undergoes a sudden variation of stresses (relaxation). The mechanical damages undergone by the rock sample can get worse due to the alteration of some minerals (mostly clay minerals) during the drying process. Thus, the mechanical representativeness of core samples is clearly questionable. It is often admitted that putting the core sample under a differential pressure P_{diff} (sometimes larger than the differential pressure in the reservoir) allows to compensate for this effect on the velocities. But what about Hertz exponents which precisely characterize the pressure sensitivity.

Some experimental work (*e.g.*, Meglis *et al.*, 1991; Rasolofosaon and Zinszner, 1989; Holt *et al.*, 1994; Schutjens *et al.*, 1995) emphasize this mechanical damage due to stress relaxation. Another illustration is the statistical comparison between Hertz exponents measured in core samples and thos measured in outcrop samples, illustrated by Figures 12 and 13. The outcrop rock samples have undergone a very slow stress relaxation (at the geological time scale), and thus have been protected from the sudden mechanical damage. One notices in Figures 12 and 13 that Hertz exponents are, in average, substantially larger in core samples than in outcrop samples, both for *P*-wave and for *S*-wave. Although there may be some bias in sampling both outcrop and core samples (complicated by recovery problem for the latter) our results statistically provide a rough but unambiguous proof of the effect of core damaging on Hertz exponents. The core damage as a result of stress unloading during coring from wells and uplifting have been pointed out by many authors (*e.g.*, Rasolofosaon and Zinszner, 1989; Holt *et al.*, 1996; Nes *et al.*, 2000).

The mechanical damage of core samples is a major issue regarding the measurement of mechanical properties in the

laboratory. Possible initiation for tackling the problem could be the study of analogue rock samples, that is to say outcrop samples geologically equivalent to the considered reservoir rocks.

CONCLUSION

The experimental results presented in this paper unambiguously demonstrate the corroboration of Biot-Gassmann equations for reservoir rocks of medium porosity, both in sandstones and in limestones, under minimum differential pressure (typically > 10 MPa) and saturated with fluids of viscosity smaller than 10^4 cP (limit of the studied range of viscosity). The uncertainty on the experimental validation is in the limit of the accuracy of the mesurements (typically a few percent on the wave moduli, that is to say half of this range for the velocities). The experimental check was done with ultrasonic waves (500 kHz). All the the theoretical developments show that the use of Biot-Gassmann theory is much more justified at smaller frequencies (*i.e.* sonic and seismic frequency bands). Thus, one can conclude that with respect to fluid substitution Biot-Gassman equations can be safely used in the interpretation of time-lapse seismic data, as illustrated by Calvert (2005).

Regarding pressure effects, the first result is that the relevant parameter is the differential pressure $P_{diff} = P_c - P_p$, that is to say the difference between the confining pressure P_c and the pore pressure P_p. More precisely, this means that *P*-wave and *S*-wave velocities only depend on the differential pressure P_{diff}, and not in an independent way on P_c and on P_p. Increasing the differential pressure P_{diff} tends to stiffen the rock by closing the mechanical defects (grain contacts, microcracks, microfractures...). The consequence on velocities and attenuations is variable according to the relative abundance of these mechanical defects in the rock sample.

Limestones are often weakly pressure dependent, whatever the pressure level. This is due to the ease with which mechanical defects can be cemented by carbonate crystals. Consolidated sandstones are often sensitive to the differential pressure P_{diff} and the unconsolidated geomaterials (sands) are very pressure sensitive.

The pressure dependence of the velocities is often well approximated by a power law. The exponent of this power law, often called the Hertz exponent, is a good way to quantify the pressure sensitivity of the rock velocities. From a practical point of view the estimation of Hertz exponent in rock samples can be jeopardized by two major factors:

– during the sample recovery the rock samples experience a sudden relaxation of the geological stresses which often tend to artificially overestimate the Hertz exponents due to the presence of the microcracks induced by the recovery process;

– the measurement of Hertz exponent involve the study of rocks under different states of differential pressures, inducing substantial variations of the attenuation/dispersion of the elastic waves in the rock samples. As a consequence, such velocity dispersion imply the frequency dependence of Hertz exponent, which is not commonly appreciated. Experimental demonstration as well as practical consequences have been recently described (Rasolofosaon and Zinszner, 2011).

REFERENCES

Anderson E.R. (1971) *Sound speed in seawater as a function of realistic temperature-salinity-pressure domains*, Naval Undersea Res. and Dev. Center, San Diego, California.

Aubry D., Biarez J., Boelle J.L., Meunier J. (1982) Identification of elastic coefficients through resonant tests of soils samples, *Soil Dynamics & Earthquake Engineering Conference*, Southampton, pp. 65-75

Bass J.D. (1995) Elasticity of minerals, glasses, and melts, in *Mineral Physics and Crystallography: A Handbook of Physical Constants*, AGU Ref. Shelf, Vol. 2, Ahrens T.J. (ed.), AGU, Washington D.C., pp. 45-63.

Batzle M., Wang Z. (1992) Seismic properties of pore fluids, *Geophysics* **57**, 1396-1408.

Biot M.A. (1941) General theory of three-dimensional consolidation, *J. Appl. Phys.* **12**, 155-164.

Biot M.A. (1956) Theory of propagation of elastic waves in a fluid saturated porous solid, I and II, *J. Acoust. Soc. Am.* **28**, 168-191.

Boelle J.L. (1983) Mesure en régime dynamique des propriétés mécaniques des sols aux faibles déformations, *Thèse*, École Centrale, Paris.

Bourbié T., Coussy O., Zinszner B. (1987) *Acoustics of Porous Media*, Technip, Paris.

Brown R.J.S., Korringa J. (1975) On the dependence of elastic properties of a porous rock on the compressibility of the pore fluid, *Geophysics* **40**, 608-616.

Cadoret T. (1993) Effet de la saturation eau/gaz sur les propriétés acoustiques des roches. Étude aux fréquences sonores et ultrasonores, *Thèse*, Université Paris 7.

Cadoret T., Marion D., Zinszner B. (1995) Influence of frequency and fluid distribution on elastic wave velocities in partially saturated limestones, *J. Geophys. Res.* **100**, B6, 9789-9803.

Calvert R. (2005) *Insights and Methods for 4D Reservoir Monitoring and Characterization*, Distinguished Instructor series n°8, SEG, Tulsa.

Carroll M.M. (1979) An effective stress law for anisotropic elastic deformation, *J. Geophys. Res.* **84**, 7510-7512.

Coussy O. (1995) *Mechanics of porous media*, John Wiley & Sons, New-York.

Daridon J.L., Lagourette B., Lagrabette A. (1999) Acoustic determination of thermodynamic properties of ternary liquid mixtures up to 150 MPa, *Phys. Chem. Liq.* **37**, 2, 137-160.

Domenico S.N. (1977) Elastic properties of unconsolidated porous sand reservoirs, *Geophysics* **42**, 7, 1339-1368.

Gassmann F. (1951) Über die elastizität poröser medien, *Vierteljahrsschrift der Naturforschenden Geselschaft in Zürich* **96**, 1-23. English translation available at: http://sepwww.stanford.edu/sep/berryman/PS/gassmann.pdf

Gurevich B. (2004) A simple derivation of the effective stress coefficient for seismic velocities in porous rocks, *Geophysics* **69**, 393-397.

Guyer R.A., Johnson P.A. (1999) Nonlinear mesoscopic elasticity: Evidence for a new class of materials, *Phys. Today* **52**, 30-35.

Hardin B.O., Richart F.E. (1963) Elastic wave velocities in granular soils, *J. Soil Mech. Found. Div. ASCE* **SM6**, 603-624.

Hardin B.O., Music J. (1965) Apparatus for Vibration of Soil Specimens During the Triaxial Test. Instruments and Apparatus for Soil and Rock Mechanics, *ASTM STP* **392**, 55-74.

Hofmann R. (2006) Frequency dependent elastic and anelastic properties of clastic rocks, *PhD Thesis*, Colorado School of Mines.

Holt R.M., Brignoli M., Fjaer E., Kenter C.J. (1994) Core damage effects on compaction behaviour, in *Proc. EUROCK'94, Rock Mechanics for Petroleum Engineering*, Balkema, Rotterdam, The Netherlands, pp. 55-62.

Holt R.M., Fjaer E., Furre A.-K. (1996) Laboratory simulation of the influence of earth stress changes on wave velocities, in *Seismic anisotropy*, Rathore J.S. (ed.), SEG, Tulsa, pp. 180-202.

Johnson P.A., Rasolofosaon P.N.J. (1996) Nonlinear elasticity and stress-induced anisotropy in rock, *J. Geophys. Res.* **101**, 3113-3124.

Lucet N. (1989) Vitesse et atténuation des ondes élastiques soniques et ultrasoniques dans les roches sous pression, *Thèse*, Université Paris 6.

Lucet N., Rasolofosaon P.N.J., Zinszner B. (1991) Sonic properties of rocks under confining pressure using the resonant bar technique, *J. Acoust. Soc. Am.* **89**, 3, 980-990.

Lucet N., Zinszner B. (1992) Effects of heterogeneities and anisotropy on sonic and ultrasonic attenuation in rocks, *Geophysics* **57**, 1018-1026.

Mavko G., Jizba D. (1991) Estimating grain-scale fluid effects on velocity dispersion in rocks, *Geophysics* **56**, 1940-1949.

Mavko G., Mukerji T., Dvorkin J. (1998) *Rock Physics Handbook*, Cambridge University Press.

Meglis I.L., Engelder T., Graham E.K. (1991) The effect of stress-relief on ambient microcrack porosity in core samples from the Kent Cliffs (New York) and Moodus (Connecticut) scientific research boreholes, *Tectonophysics* **186**, 163-173.

Nes O.-M., Holt R.M., Fjaer E. (2000) The reliability of core data as input to seismic reservoir monitoring studies, *Proceedings of SPE European Petroleum Conference*, Paris, *SPE paper* 65180.

Nur A., Byerlee J.D. (1971) An exact effective stress law for elastic deformation of rocks with fluids, *J. Geophys. Res.* **76**, 6414-6419.

Plantier F., Daridon J.L., Lagourette B. (2002) Nonlinear parameter (B/A) measurement in methanol,1-butanol and 1-octanol for different pressure and temperatures, *J. Phys. D: Appl. Phys.* **35**, 1063-1067.

Pouet B., Rasolofosaon P.N.J. (1993) Measurement of broadband intrinsic ultrasonic attenuation and dispersion in solids with laser techniques, *J. Acoust. Soc. Am.* **93**, 3, 1286-1292.

Rasolofosaon P.N.J., Zinszner B. (1989) Effect of *in-situ* stress relaxation on P- and S-wave ultrasonic anisotropy, in *Rock at great depth*, Fourmaintraux D., Maury V. (eds), *Proceedings of International Symposium on Rock Mechanics Held in Pau*, France, August, 1, pp. 305-312.

Rasolofosaon P.N.J., Lucet N., Zinszner B. (2008) Petroacoustics of carbonate reservoir rocks, *Lead. Edge* **27**, 8, 1034-1039.

Rasolofosaon P.N.J., Yin H. (1996) Simultaneous characterization of anisotropy and nonlinearity in arbitrary elastic media, in *Seismic Anisotropy*, Fjaer E., Holt R.N., Rathore J.S. (eds), *Transactions of the 6th Int. Workshop on Seismic Anisotropy*, SEG, Tulsa.

Rasolofosaon P.N.J., Zinszner B.E. (2003) Petroacoustic characterization of reservoir rocks for seismic monitoring studies, *Oil Gas Sci. Technol.* **58**, 6, 615-635.

Rasolofosaon P.N.J., Zinszner B. (2004a) Laboratory petroacoustics for seismic monitoring feasibility study, *Lead. Edge* **23**, 3, 252-258.

Rasolofosaon P.N.J., Zinszner B. (2004b) *Méthode de mesure des paramètres élastiques d'un matériau poreux*, Brevet français FR2856795.

Rasolofosaon P., Zinszner B. (2011) Frequency dependence of Hertz exponent of Velocity-Pressure power law in Petroelastic Models and Practical consequences, *73rd EAGE Conference and Exhibition, Vienna, Paper Number D008.*

Robin P.Y.F. (1973) Note on effective pressure, *J. Geophys. Res.* **78**, 2434-2437.

Schutjens P.M.T.M., Hausenblas M., Dijkshoorn M., van Munster J.G. (1995) The Influence of Intergranular Microcracks on the Petrophysical Properties of Sandstone – Experiments to Quantify Effects of Core Damage, *SCA Conference*, Paper Number 9524.

Tamura K., Murakami S., Fukumori M., Akagi Y., Kawasaki Y. (1994) Thermodynamic properties of binary mixtures: Hexamethylphosphoric triamide + a polar liquid at 25°C, *J. Solution Chem.* **23**, 263-273.

Tarif P. (1986) Mesure de l'atténuation des ondes compressionelles ultrasoniques dans les roches : application à la mesure de l'anisotropie d'atténuation, *Thèse*, Université Pierre et Marie Curie, Paris 6.

Thompson M., Willis J.R. (1991) Reformation of the equations of anisotropic poroelasticity, *J. Appl. Mech.* **58**, 612-616.

Walsh J.B., Brace W.F. (1966) Cracks and pores in rocks, *Proc. 1st Congress Int. Soc. of Rock Mechanics*, Lisbonne, 1, pp. 643-646.

Wang H.F. (2000) *Theory of Linear Poroelasticity*, Princeton University Press, Princeton, NJ.

Winkler K.W. (1979) The effects of pore fluids and frictional sliding on seismic attenuation, *PhD Thesis*, Stanford University.

Zimmerman R.W. (1991) *Compressibility of sandstones*, Elsevier.

Zinszner B., Johnson P.A., Rasolofosaon P.N.J. (1997) Influence of change in physical state on elastic nonlinear response in rock: Significance of effective pressure and water saturation, *J. Geophys. Res.* **102**, B4, 8105-8120.

Zinszner B., Pellerin F.M. (2007) *A Geoscientist's Guide to Petrophysics*, Technip, Paris.

Final manuscript received in November 2011
Published online in April 2012